Oxidation of *o*-xylene to phthalic anhydride on Sb-V/ZrO_2 catalysts

C.L. Pieck*, S. del Val, M. López Granados, M.A. Bañares, and J.L.G. Fierro

Instituto de Catálisis y Petroleoquímica, CSIC, Campus Cantoblanco, E-28049 Madrid, Spain

Received 14 August 2002; accepted 17 April 2003

Zirconia-supported and bulk-mixed vanadium–antimonium oxide catalysts were used for the oxidation of *o*-xylene to phthalic anhydride. X-ray diffraction, Raman spectroscopy and photoelectron spectroscopy were used for characterization. It was found that vanadium promotes the transition of tetragonal to monoclinic zirconia. The simultaneous presence of Sb and V on zirconia at low coverage led to a preferential interaction of individual V and Sb oxides with the zirconia surface rather than the formation of a binary Sb-V oxide, while at higher Sb-V contents the formation of $SbVO_4$ took place. Sb-V/ZrO_2 catalysts showed high activity for *o*-xylene conversion and better selectivity to phthalic anhydride as compared to V/ZrO_2 catalysts. However, their selectivity to phthalic anhydride was poor in comparison to a V/TiO_2 commercial catalyst. The improved selectivity of the Sb-containing catalysts is attributed to the blocking of non-effective surface sites of ZrO_2, the decrease of the total amount of acid sites and the formation of surface V-O-Sb-O-V structures.

KEY WORDS: o-xylene oxidation; phthalic anhydride; Sb-V/ZrO_2 catalysts.

1. Introduction

Aromatic carboxylic anhydrides are produced in large quantities through the partial oxidation of hydrocarbon feedstocks; in particular, phthalic anhydride from ortho-xylene. Phthalic anhydride is useful for reactions with alcohols, such as oxo-alcohols, to form the corresponding phthalic anhydride alcohol esters, which are used as plasticizers and lubricants. Phthalic anhydride is obtained industrially via single-stage selective oxidation of *o*-xylene with a 100% conversion and a selectivity to phthalic anhydride of 80% [1,2]. Some byproducts, such as CO and CO_2, are formed during the reaction. The catalyst used in the process—VO_x/TiO_2 anatase—has been explored with regard to its structure–activity relationships [3–6] and reaction mechanism [1,2].

A previous work has revealed that the VO_x/ZrO_2 system is active for *o*-xylene oxidation to phthalic anhydride [7]. Nevertheless, surface V is excessively active and drives the formation of deep oxidation products (CO and CO_2). We have also reported that activity decreases with V-loading while selectivity to phthalic anhydride passes through a maximum [7].

In this paper, we undertake the study of V-Sb/ZrO_2 catalysts for oxidation of *o*-xylene to phthalic anhydride. We have been mainly motivated by the appearance of many patents that point out the importance of Sb_2O_3 in improving the performance of the V_2O_5/TiO_2 (anatase) catalysts [8–12] and by the chemical similarity between TiO_2 and ZrO_2. Zr and Ti are column neighbors in the periodic table with the d^2s^2 electronic configuration. Both ZrO_2 and TiO_2 oxides have d^0 configuration in their outer shell and they tend to develop unstoichiometry (oxygen deficiency) and *n*-type semiconductivity. Redox interactions between catalyst surface species and adsorbates through the conduction band have been postulated mainly for TiO_2 catalysts, e.g., V_2O_5-TiO_2 catalysts, but also for ZrO_2 catalysts, e.g., WO_3-ZrO_2 or SO_4^{2-}-ZrO_2. The successful oxidation of *o*-xylene to phthalic anhydride has indeed been reported for V_2O_5/ZrO_2-TiO_2 catalysts [13]. Zirconia itself has long attracted the interest of the scientific community for different catalytic uses, including redox reacting systems: isomerization of light hydrocarbons [14], toluene oxidation [15], oxidative dehydrogenation [16], three-way catalysts [17], fuel cells and electrocatalysis [18], etc.

Regarding the effect of Sb, though the information in patents is most of the time scarce and deceiving, the agreement between many authors about the positive effect of Sb drew our attention. It has been reported that total oxidation occurs over strong acid sites [19] and Chiang and Lee [20] have proved by means of NH_3-TPD experiments that Sb reduces the acidity of V-supported catalysts. We expected Sb to improve the selectivity of V/TiO_2 catalysts since Spengler *et al.* [21] have recently shown that in the case of the oxidation of *o*-xylene to phthalic anhydride there exists an improvement in the selectivity to anhydride when Sb is added to the V_2O_5/TiO_2 catalyst owing to the intercalation of Sb into V-O-V-O-V clusters. They report that V-O-V-O-V species lead to overoxidation, Sb-O-Sb-O-Sb species are

* To whom correspondence should be addressed.
E-mail: pieck@fiqus.unl.edu.ar

1011-372X/03/0700–0027/0 © 2003 Plenum Publishing Corporation

inactive, and isolated V-O-Sb-O-V species are ideal for selective (*o*-xylene) oxidation.

Our present study on the Sb-V_2O_5-ZrO_2 system is mainly aimed at obtaining fundamental information on the redox activity of the V_2O_5-ZrO_2 catalyst, its selectivity to mild oxidation products and the influence of Sb loading. Catalytic reaction tests have been complemented with XRD and Raman spectra in order to characterize bulk and surface species.

2. Experimental

2.1. Catalyst preparation

The ZrO_2 support was prepared from a commercial $Zr(OH)_4$ sample (MEL Chemicals) by calcination in air at 650 °C for 4 h. The TiO_2 (anatase) was supplied by Than and Mulhouse (pigment grade, BET surface area 10 m^2/g). The catalysts' preparation procedure has been described elsewhere [22]. Basically, ternary Sb-V/ZrO_2 systems were prepared by impregnating the support (ZrO_2) with aqueous solutions of the two oxides. 200 cm^3 of distilled water were acidified to a pH value of 2 with nitric acid. Then, tartaric acid was added (9 g), along with an adequate amount of Sb_2O_3. The Sb_2O_3 was dissolved while stirring gently at 80–90 °C. Then the solution was cooled to room temperature and NH_4VO_3 was added and dissolved. Finally, the support was added (4 g) and the solution was vacuum-dried in a rotary evaporator at (80 °C, 0.3 atm) until a dried powder was obtained. The powder was dried in an oven at 120 °C overnight and was finally calcined in air at 650 °C for 4 h. Two series of catalysts were prepared. One series had a fixed Sb/V atomic ratio and different loadings of (V + Sb). The other series had a constant loading of (V + Sb) and different Sb/V atomic ratios. The catalysts of the zirconia-supported series were named xSb_yV/ZrO_2. x is the (Sb + V) content expressed in nominal monolayers and y is the Sb/V atomic ratio. The monolayer content was calculated by considering the surface density of (Sb + V) species and the original surface area of the zirconia support. The V/ZrO_2, V/TiO_2 and Sb/ZrO_2 samples were prepared in a similar way. Bulk $[Sb\text{-}V]^r$ samples were prepared by mixing aqueous solutions of Sb_2O_3 (in tartaric acid) with NH_4VO_3 in the appropriate concentration to yield atomic ratios $r = Sb/V$ of 0.5, 1 and 3. Drying and calcination steps were the same as above. Reference ZrV_2O_7 was also prepared, as described elsewhere [22]. A stoichiometric amount of $Zr(OH)_4$ was added to a solution of NH_4VO_3 to obtain an atomic ratio of $V/Zr = 2$. Excess water was removed in a rotary evaporator at 80 °C. Then, the dried precursor was kept in an oven at 120 °C for 16 h and finally calcined at 650 °C for 24 h. Table 1 shows a list of catalysts used in this work.

Table 1
Catalysts composition (wt%), specific surface area and Sb/V surface atomic ratios (from XPS data)

Catalysts	V_2O_5 (%)	Sb_2O_3 (%)	BET area (m^2/g)	Atomic ratio	
				$(Sb/V)_{XPS}$	$(Sb/V)_{bulk}$
ZrO_2	–	–	86		
ZrV_2O_7			< 1		
Sb/ZrO_2	–	13.7	64	–	–
V/TiO_2	7.16	–	9	–	–
V/ZrO_2	9.05	–	10	–	–
$2Sb_{0.5}V/ZrO_2$	10.71	8.58	12	0.29	0.50
$2Sb_1V/ZrO_2$	7.90	12.67	17	0.89	1.00
$2Sb_3V/ZrO_2$	4.40	21.11	28	2.91	2.99
$0.5Sb_3V/ZrO_2$	1.09	5.23	69	2.04	2.99
$1Sb_3V/ZrO_2$	2.17	10.46	52	2.04	3.01
Bulk catalysts					
$[Sb\text{-}V]^{0.5}$			7	0.88	0.50
$[Sb\text{-}V]^1$			6	1.19	1.00
$[Sb\text{-}V]^3$			5	3.34	3.00

2.2. Catalyst characterization

Chemical analysis of the samples to determine V, Sb, Ti and Zr composition was carried out by ICP using Perkin-Elmer Optima 3300 DV apparatus. The surface area of the catalysts was calculated from nitrogen adsorption isotherms (−196 °C) using the BET method. X-ray diffraction patterns were recorded in a Siemens Krystalloflex D-500 diffractometer using CuKα radiation ($\lambda = 0.15418$ nm) and a graphite monochromator. Raman spectra were recorded on a Renishaw System 1000 apparatus equipped with a single monochromator, a CCD detector refrigerated at −73 °C and a holographic super-Notch filter. Spectra were obtained with a 514-nm excitation line (9 mW) under dehydration conditions (dry air at 120 °C) in a hot stage device (Linkam TS-1500). Photoelectron spectra were recorded in a Fisons Escalab 200R apparatus, equipped with a hemispherical electron analyzer and an Mg Kα (1253.6 eV) X-ray source. Residual pressure in the analysis chamber was less than 5.10^{-9} mbar during data acquisition. The binding energy of the C_{1s} peak of adventitious carbon at 284.9 eV was taken as internal standard. Temperature-programmed-desorption of ammonia with mass spectrometry analysis (TPD-MS-NH_3) was performed in a flow equipment connected in series to a mass spectrometer (Balzers QMG 421C quadrupole). The samples were first treated at 500 °C with a mixture of 8% oxygen in He for 2 h. Then, NH_3 was adsorbed at 120 °C for 150 min from a flowing mixture of 5% NH_3 in He. Finally, the temperature was raised at a rate of 10 °C/min and a stream of pure He was injected into the reactor. The desorbed species were analyzed on-line.

2.3. Catalytic activity

Catalytic activity measurements were carried out in a plug-flow glass fixed-bed reactor heated by a cylindrical oven. The apparatus has been previously described [23]. The reactor catalyst load consisted of 0.06 g of catalyst diluted with carborundum (0.42–0.50 mm particles) in a 1 : 7 weight ratio. The contact time (W/F) was 42 g · s/L. The molar concentrations of *o*-xylene and oxygen in the feed were 0.8 and 20.8% respectively (78.4% nitrogen). The inlet lines were heated to 180 °C in order to ensure the evaporation of alkyl aromatics. An ice-bath trap was placed between the GC and the reactor outlet to condense part of the products. The lines connecting the reactor and the trap were heated to 250 °C. The temperature of the bottom of the reactor, downstream the catalyst bed, was higher than 350 °C. A gas chromatograph (GC) (Varian Star 3400CX) was connected on-line with the reactor outlet in order to analyze volatile fractions and permanent gases. The rest of the products, which were condensed in the ice-trap, were dissolved in acetone and analyzed by syringe injection. The GC was equipped with thermal conductivity and flame ionization detectors. Organic products were separated by an RTX-5 capillary column, and O_2, H_2O, CO and CO_2 were separated by two packed columns connected in series (HayeSep D and 5 A molecular sieve).

3. Results and discussion

Table 1 shows the composition (wt%), specific surface area and Sb/V atomic ratio of the catalysts, as obtained by XPS. The bulk [Sb-V] catalysts had low BET areas that decreased with the Sb/V atomic ratio. A similar trend was reported by Chian and Lee [20]. Regarding the surface Sb/V atomic ratio, bulk catalysts showed a surface enrichment in Sb with respect to the theoretical Sb/V ratio. In the case of the supported catalysts, it can be seen that the addition of V or Sb to the zirconia support decreased the surface area. This effect was more pronounced in the case of V/ZrO_2. BET areas of the Sb-V/ZrO_2 series had intermediate values, and the specific surface area decreased when the Sb/V atomic ratio increased. The V/TiO_2 catalyst had a small surface area. The incorporation of V to TiO_2 (anatase) produced only a little decrease in the BET area (from 10 to 8 m^2/g), which was probably due to V blocking of the anatase pores.

The XPS intensity ratios V/Zr, V/Ti and Sb/Zr of the supported catalysts had higher values than that corresponding to the bulk one, as expected for supported oxides. The supported catalysts also exhibited lower Sb/V atomic ratios than the theoretical value, indicating a surface enrichment in V. This phenomenon can be explained taking into account the stronger interaction of vanadia on a zirconia support.

Figure 1 shows the XRD patterns of the V/TiO_2 (anatase), Sb/ZrO_2, V/ZrO_2 and bulk catalysts. The XRD pattern of the ZrO_2 support is also included for comparison. It is clear from the diffraction at 30.5° that the ZrO_2 support had a fluorite-type structure. The absence of diffractions peaks at 28.2 and 31.5° further confirms that the monoclinic phase was not formed [24]. The diffractograms of the V/ZrO_2 catalyst indicate that the incorporation of vanadium induces a transformation of the ZrO_2 phase. The 30.5° peak disappears while the peaks due to the monoclinic phase appear. The pattern is completed by other peaks 16°, 20°, 22.5° and 24.8°, characteristic of the ZrV_2O_7 phase [25]. The tetragonal phase is still present in the Sb/ZrO_2 catalyst, while the development of the monoclinic phase is only incipient (reflection peaks at 28.2 and shoulder at 31.5°). The V/TiO_2 catalyst only yielded diffraction peaks at 25.3, 37.0, 37.8, 38.6, 48.0, 53.9, 55.1, 62.7 and 68.8°, which can be attributed to the anatase phase of TiO_2 [26]. No diffraction peaks due to V_2O_5 crystals or to the rutile phase of TiO_2 could be found.

The diffraction pattern of the bulk $[Sb\text{-}V]^1$ catalyst had peaks at 27.5, 35.3, 39.3, 40.5, 53.8, 56.1, 65.1 and 68.7°, which correspond to the $SbVO_4$, rutile-type phase [27–29]. Two very little peaks at 25.8° and 29° could also be distinguished and were readily attributed to the Sb_2O_4 cervantite phase [30]. Regarding the $[Sb\text{-}V]^3$ sample, it is evident that the $SbVO_4$ phase is accompanied by Sb_2O_4 and α-Sb_2O_4 cervantite because the diffraction angles at 25.8 and 29° are more intense. The

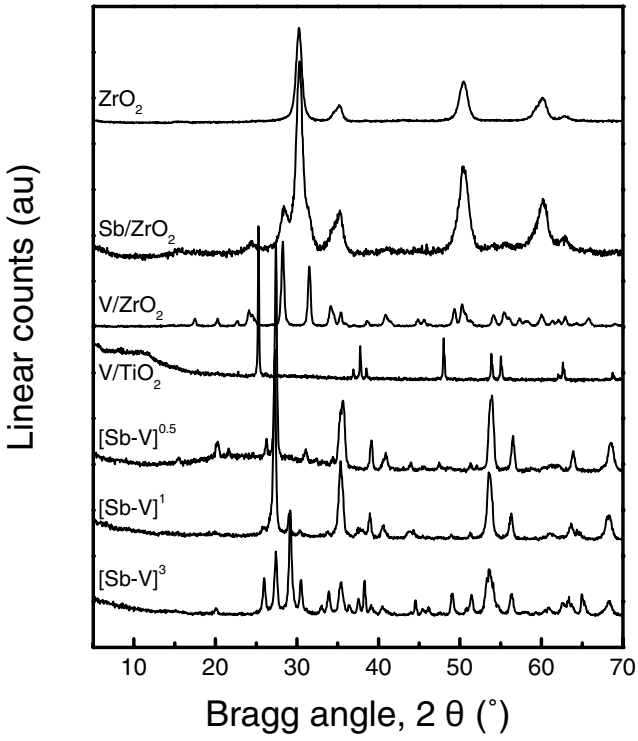

Figure 1. X-ray diffraction spectra of unsupported [Sb-V] catalyst, ZrO_2, V/ZrO_2, Sb/ZrO_2 and V/TiO_2 catalysts.

$[Sb\text{-}V]^{0.5}$ samples has peaks at 15.4, 20.3 and 31.0° due to V_2O_5 crystallites [31] and peaks corresponding to a $SbVO_4$ phase. The XRD data of the bulk catalysts are in agreement with those reported by Nilsson *et al.* [32]. They reported that bulk Sb-V with high Sb/V ratio exhibited a $SbVO_4$ rutile-type structure and that the excess of Sb produced superficial α-Sb_2O_4 while catalysts with lower Sb/V showed crystalline V_2O_5.

Figure 2 shows the XRD spectra of the zirconia-supported Sb-V oxide catalysts. The $0.5Sb_3V/ZrO_2$ and $2Sb_{0.5}V/ZrO_2$ catalysts display both tetragonal and monoclinic phases but the tetragonal former predominates (peak at 30.5°). Only the tetragonal phase is developed in the catalysts with higher Sb contents. The XRD spectra of the $2Sb_{0.5}V/ZrO_2$ and $0.5Sb_3V/ZrO_2$ catalysts show some little diffraction peaks at 16, 20, 22.5 and 24.8°, characteristic of ZrV_2O_7. The $2Sb_{0.5}V/ZrO_2$ catalyst also exhibits some peaks that could be attributed to V_6O_{13} [33] and the $2Sb_1V/ZrO_2$ catalysts some other peaks related to the VO_2 paramontroseite phase [34]. The stabilizing effect of the tetragonal phase of ZrO_2 at high Sb-V contents suggests the existence of some interaction between the two oxides, although no zirconia with Sb and V can generate the diffraction pattern of the $SbVO_4$ phase. Therefore, if $SbVO_4$ was formed in these samples, it must be distributed in very small domains that cannot be detected by X-ray diffraction.

The Raman spectra of bulk Sb-V catalysts, as well as those of the ZrO_2, Sb/ZrO_2, V/TiO_2 and V/ZrO_2 samples, are shown in figure 3. The results confirm that ZrO_2 support has a tetragonal structure because the characteristic peaks of this phase can be seen at 143, 263, 325, 474, 608 and 640 cm^{-1} [35]. The incorporation of vanadium to zirconia promotes the appearance of the monoclinic phase. The spectrum of V/ZrO_2 has bands related to this phase at 175, 190 and 477 cm^{-1}. It must also be noted that the V/ZrO_2 spectra also has a broad band at 780 and 990 cm^{-1} due to ZrV_2O_7 [22] and bands at 143, 283, 302, 405, 526, 698 and 994 cm^{-1} corresponding to crystalline V_2O_5 [36–38]. The Raman spectra of V/TiO_2 show anatase bands at 143, 199, 395, 516 and 638 cm^{-1} [38,39] and V_2O_5 bands 144, 196, 284, 304, 406, 484, 528, 702 and 996 cm^{-1} [36–38]. Finally, the spectrum of bulk $[Sb\text{-}V]^3$ oxide has bands at 190 and 397 cm^{-1}, associated with α-Sb_2O_4 [32], and a broad peak at 750–950 cm^{-1}, presumably due to the presence of rutile-type phase of $SbVO_4$ [32]. On the contrary, $[Sb\text{-}V]^{0.5}$ and $SbVO_4$ (i.e., $[Sb\text{-}V]^1$) showed peaks at 143, 283, 523, 694 and 994 cm^{-1}, related to V_2O_5.

Figure 4 shows the Raman spectra of the $Sb\text{-}V/ZrO_2$ catalysts. The spectrum of $2Sb_3V/ZrO_2$ exhibits bands at 452 cm^{-1} and 750–950 cm^{-1} (broad), which can be ascribed to the appearance of the $SbVO_4$ phase, and bands at 263, 325, 472 and 640 cm^{-1}, attributed to the tetragonal phase of zirconia. The spectra of $1Sb_3V/ZrO_2$ and $0.5Sb_3V/ZrO_2$ exhibit bands due to Sb_2O_4 (190 and 400 cm^{-1}), dispersed vanadium oxide (1030 cm^{-1}), $SbVO_4$ (750–950 cm^{-1} and 452 cm^{-1}) and the monoclinic phase of ZrO_2. V forms ZrV_2O_7 (peaks

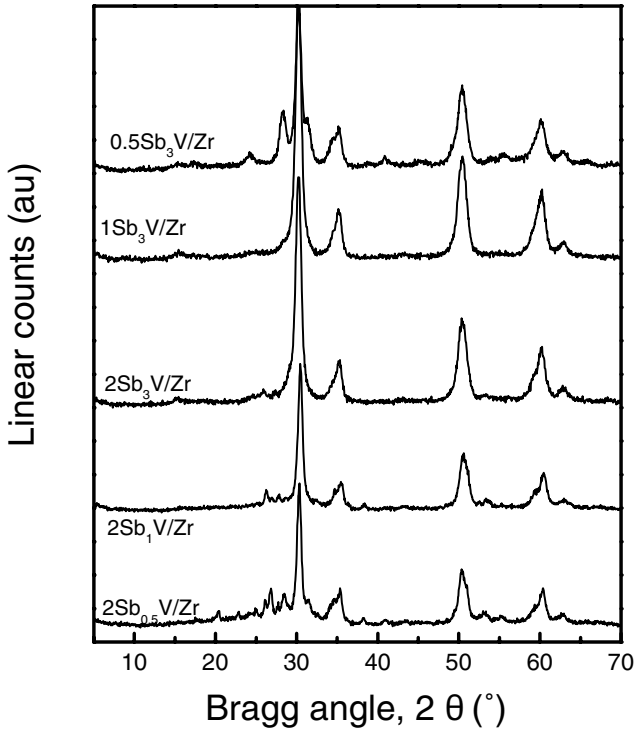

Figure 2. X-ray diffraction spectra of supported $Sb\text{-}V/ZrO_2$ catalyst.

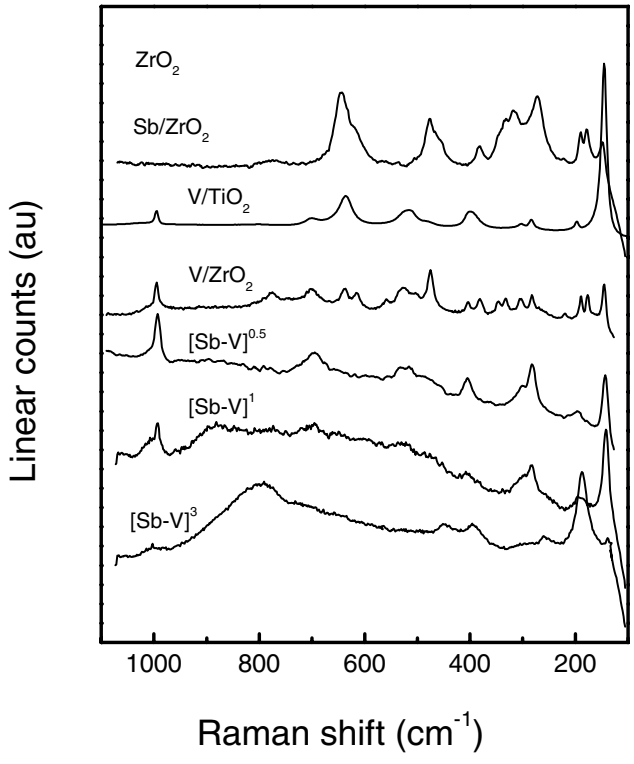

Figure 3. Raman spectra of dehydrated unsupported [Sb-V] catalyst, ZrO_2, V/ZrO_2, Sb/ZrO_2 and V/TiO_2 catalysts.

at 780 and 990 cm^{-1}) [22] since the Sb/V atomic ratio decreased for $2Sb_{0.5}V/ZrO_2$ catalyst. $2Sb_1V/ZrO_2$ exhibits a large and broad Raman band between 900 and 1000 cm^{-1}, which could be ascribed to the $SbVO_4$ phase [32].

It can be concluded from the results that the incorporation of Sb modified the tetragonal structure of the ZrO_2 support and decreased the specific area moderately. The addition of V promoted the tetragonal-to-monoclinic transition of the support, a great surface area reduction and the formation of ZrV_2O_7. On the other hand, the simultaneous promotion with Sb and V beyond monolayer coverage stabilized the tetragonal phase and minimized the formation of the ZrV_2O_7 phase. At low Sb + V loading, dispersed V oxide species were present. These surface species promoted the tetragonal-to-monoclinic transition of the support. At high Sb + V loading, the interaction between V and Sb limited the capacity of V to transform the ZrO_2 support because of the formation of $SbVO_4$. Moreover, the excess of V or Sb leads to formation of surfaces oxides of V or Sb on the catalyst. The bulk catalysts had a bulk $SbVO_4$ rutile structure with Sb_2O_4 or V_2O_5 oxides on the surface depending on the Sb/V ratio.

With respect to the catalytic activity tests, a preliminary screening of the reaction temperature was first done in order to find the optimum one. A value was searched that could give a conversion close to 100% with good selectivity to phthalic anhydride. At low conversion the selectivity was poor. Too many intermediate products were found among the reaction products. Total conversion conditions had to be carefully tuned because they could lead to deep oxidation of the hydrocarbons to CO and CO_2. This usually happens when the temperature is too high.

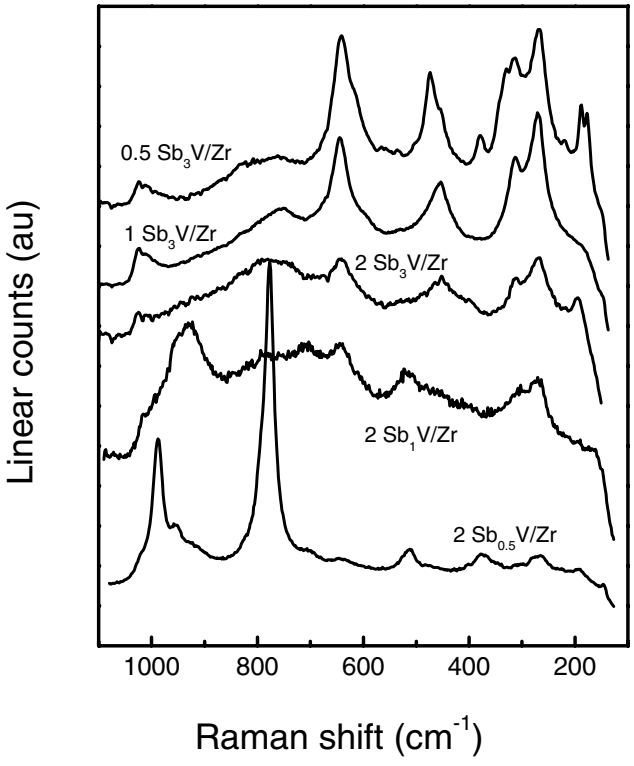

Figure 4. Raman spectra of dehydrated supported Sb-V/ZrO_2 catalyst.

Some heavily oxidized products were detected, e.g., *o*-, *p*-methyl-diphenyl methanone, diphenyl methanone or other high boiling point products. Their concentration was only important at low values of *o*-xylene conversion (ZrO_2 and ZrV_2O_7 at 400 °C and Sb/ZrO_2 at 440 °C). These products are indicated as "others" in tables 2 and 3. Table 2 shows activity and selectivity values corresponding to the bulk catalysts, the support and the reference compound ZrV_2O_7. Some amounts of maleic anhydride and *o*-toluic acid were formed during the reaction, but except for ZrV_2O_7, the selectivity to phthalic anhydride was small (< 3%). The activity of ZrV_2O_7 was similar to that of the ZrO_2 support. The latter produced mainly deep oxidation products, while ZrV_2O_7 exhibited a lower activity for deep oxidation, selectivity to phthalic anhydride being similar. In the case of the bulk Sb-V catalysts, it was observed that the activity decreased as the Sb/V atomic ratio was increased, but the selectivity to phthalic anhydride remained unaffected. It is important to stress that the catalyst with ratio Sb/V = 3 had the highest selectivity to intermediate products and the lowest selectivity to CO_x products. Probably this catalyst would have had more selectivity at phthalic anhydride at higher conversion values. This fact can be related to the different surface species. In the case of the bulk catalysts $[Sb\text{-}V]^{0.5}$ and $[Sb\text{-}V]^1$, the Raman results point to the presence of surface vanadium oxide, which seems to be active for the oxidation of *o*-xylene. In the case of the $[Sb\text{-}V]^3$ catalyst, the formation of V_2O_5 was not detected and the excess of Sb led to the formation of surface α-Sb_2O_4, but it is not active for the reaction. According to Spengler *et al.* [21], V-O-Sb-O-V species are ideal for selective *o*-xylene oxidation. This structure was formed in all the bulk Sb-V catalysts but only in the case of $[Sb\text{-}V]^3$, the V_2O_5 crystals responsible of CO_x formation were absent.

It can be seen in table 2 that the V/TiO_2 catalyst, which had a similar composition as the commercial ones, had both higher activity and selectivity to phthalic anhydride than the bulk Sb-V catalysts and the V/ZrO_2 catalyst. This better performance must be due to the different interface on which surface vanadia species disperse, i.e., the anatase interface [24]. The poor performance of the V/ZrO_2 catalyst as compared to V/TiO_2 can also be explained by taking into account that when supported on ZrO_2, V reacted with the support to form ZrV_2O_7, a compound with little activity and little selectivity to phthalic anhydride.

Figure 5 shows values of conversion of *o*-xylene and selectivities to phthalic anhydride, CO_2, CO, phthalide and *o*-tolualdehyde as a function of the Sb-V loading for the catalysts supported on ZrO_2 with an atomic ratio of

Table 2
Activity and selectivity of bulk Sb-V catalysts, zirconia, zirconia vanadate and V/TiO_2, during the oxidation of phthalic anhydride

Catalyst	Temp. (°C)	Conversion (%)	Selectivity							
			PA	CO_2	CO	*o*-t	ph	MA	*o*-t A	Others
$[Sb\text{-}V]^{0.5}$	420	97.0	48.0	33.2	13.3	0.8	1.8	2.8	0.0	0.1
$[Sb\text{-}V]_1$	420	95.0	50.0	33.7	11.6	1.1	1.1	2.4	0.1	0.0
$[Sb\text{-}V]^3$	440	57.0	49.0	23.2	4.0	14.4	6.9	1.2	0.5	0.8
ZrV_2O_7	400	23.9	6.7	26.1	0.0	22.2	3.5	0.6	9.5	31.4
V/TiO_2	380	85.5	61.8	23.9	5.5	4.3	2.7	1.2	0.0	0.6
ZrO_2	400	25.7	4.4	70.0	0.0	12.7	5.0	1.7	0.0	6.2

Note: PA: phthalic anhydride, *o*-t: *o*-tolualdehyde, ph: phthalide, MA: maleic anhydride, *o*-t A: *o*-toluic acid.

$Sb/V = 3(xSb_3V/ZrO_2)$. The ZrO_2 support exhibited both low conversion and selectivity towards the desired product (phthalic anhydride). Conversion and selectivity to phthalic anhydride increased with the loading with Sb-V. Selectivity to CO remained almost constant and selectivity to CO_2 decreased upon increasing the Sb-V loading. This result can be explained if we consider the surface structure of the Sb-V/ZrO_2 catalysts, as elucidated by our Raman and XRD results. At low Sb-V loadings, zirconia Sb and V surface dispersed oxide species are formed. Surface VO_x is very active and highly selective to CO and CO_2 [7]. At coverage values higher than one monolayer, Sb and V coordinate to form $SbVO_4$ at the expense of surface VO_x species [22]. In the case of the V_2O_5/TiO_2 (anatase) catalyst, it has been reported that exposed titania sites may lead to complete oxidation of C_8-oxygenates [40]. This effect would account for the increase in selectivity to phthalic anhydride with the increase in Sb-V loading. Another factor contributing to the improvement in selectivity is the formation of Sb-V loading mixed oxides at high loading values of V and Sb. According to Spengler *et al.* [21] the V-O-Sb-O-V structures are more selective than the V-O-V-O-V ones. Moreover, the Sb promotion decreases the acidity of the catalysts, as it can be inferred from the results of table 3. The reduced surface acidity could lead to a weaker interaction of the catalyst with *o*-xylene, the reaction intermediates and the products, and hence to a shorter residence time on the surface. It has been reported previously that strong acid sites are responsible for over oxidation [19].

The results of table 4 indicate that the V/ZrO_2 catalyst is more active and selective towards phthalic anhydride than the Sb/ZrO_2 catalyst. Moreover, when the selectivity to phthalic anhydride and the total conversion of the Sb/ZrO_2 and ZrO_2 samples are compared, it results that the support is more active and selective and that their selectivity to CO_x is almost the same. It therefore seems that Sb blocks some active sites of the ZrO_2 support and increases the selectivity to anhydride by destroying those responsible for deep oxidation.

Table 3
Total acidity of the supported catalysts as obtained by the NH_3-TPD technique

Catalyst	NH_3 (a.u./m^2)
ZrO_2	0.81
Sb/ZrO_2	0.47
V/ZrO_2	2.70
$0.5Sb_3V/ZrO_2$	1.25
$1Sb_3V/ZrO_2$	1.41
$2Sb_3V/ZrO_2$	1.14

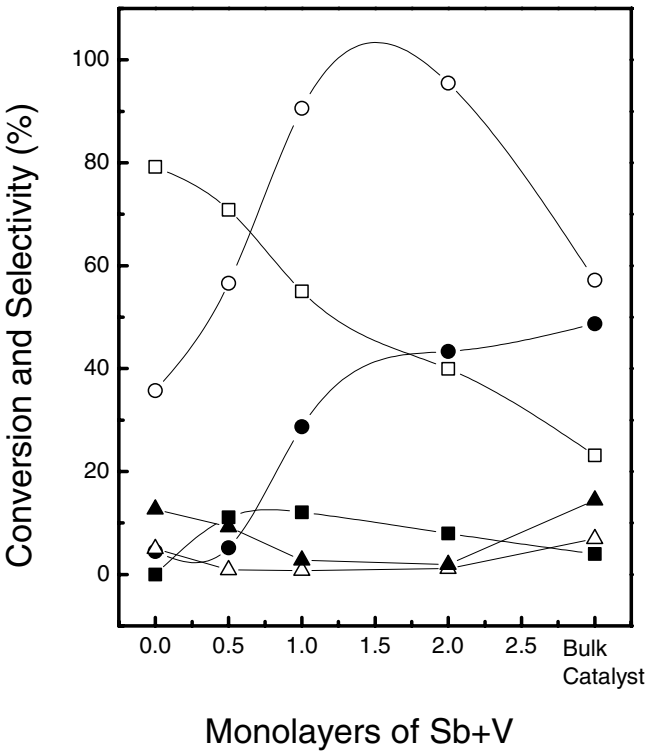

Figure 5. Catalytic activity data for the reaction of *o*-xylene oxidation as a function of the Sb + V monolayers supported on ZrO_2. (○), conversion; (●), selectivity to phthalic anhydride; (□), selectivity to CO; (△), selectivity to phthalide; (▲), Selectivity to *o*-tolualdehyde. Reaction temperature: 440 °C.

Table 4
Conversion and selectivity obtained in the oxidation of *o*-xylene. Supported catalysts with two Sb-V monolayers

Catalyst	Temp. (°C)	Conversion (%)	Selectivity							
			PA	CO_2	CO	*o*-t	ph	MA	*o*-tA	Others
$2Sb_{0.5}V/ZrO_2$	390	94.9	48.3	34.0	11.9	2.3	1.5	1.9	0.0	0.1
$2Sb_1V/ZrO_2$	400	96.2	43.5	37.1	15.3	0.4	0.5	3.2	0.0	0.0
$2Sb_3V/ZrO_2$	440	95.5	43.3	39.9	8.0	1.9	1.1	5.7	0.0	0.1
Sb/ZrO_2	440	13.2	0.9	59.1	9.9	20.8	2.9	1.1	0.0	5.3
V/ZrO_2	410	99.2	35.2	45.8	15.7	1.2	0.7	1.4	0.0	0.0

Note: PA: phthalic anhydride, *o*-t: *o*-tolualdehyde, ph: phthalide, MA: maleic anhydride, *o*-t A: *o*-toluic acid.

Since the best conversion and selectivity values to phthalic anhydride were obtained with the catalyst with two monolayers, we decided to study the influence of the Sb/V ratio on a series of catalysts with a constant loading of two Sb + V monolayers. The reaction temperature was varied in order to reach the same conversion value. Table 4 shows that when the Sb/V ratio was increased the catalyst became less active, in agreement with the lower activity of Sb, while selectivity to phthalic anhydride decreased slightly. Again, as the Sb/V ratio was increased, the excess of Sb inhibited the formation of surface vanadia species and decreased the activity to CO_x products. The results of figure 5 indicate that the bulk catalyst (Sb/V = 3) is less active than the supported catalyst with two monolayers. This result seems to be related to the difference in specific surface area.

4. Conclusions

Supported Sb-V/ZrO_2 and bulk Sb-V catalysts have the capacity to selectively transform *o*-xylene into phthalic anhydride. However, they require a higher operation temperature than a commercial V_2O_5/TiO_2 catalyst, if a similar conversion value is to be achieved. Their selectivity to phthalic anhydride is also lower. The incorporation of Sb to the V_2O_5/ZrO_2 catalyst improves its selectivity and the effect seems to be related to the three causes: (a) blocking of non-selective surface sites in zirconia, (b) formation of superficial V-O-Sb-O-V species, and (c) the decrease of the total amount of acid sites.

Acknowledgments

C.L.P. thanks the Spanish Ministry of Education for a grant to fund his stay in Spain. This research was partly funded by the EU under Project BE-1169. CICYT grant IN96-0053 funded the acquisition of the Raman spectrometer. Thanks are due to Professor M.A. Vicente for XRD experiments.

References

[1] V. Nikolov, D. Klissurski and N. Anastasov, Catal. Rev. Sci. Eng. 33 (1991) 319.
[2] C.R. Dias, M.F. Portela and G.C. Bond, Catal. Rev. Sci. Eng. 39 (1997) 169.
[3] G.C. Bond, J.P. Zurita and S. Flamers, Appl. Catal. 27 (1986) 353.
[4] R.S. Saleh, I.E. Wachs, S.S. Chan and C.C. Chersich, J. Catal. 98 (1986) 102.
[5] J.C. Vedrine (ed.), Catal. Today 20 (1994).
[6] G.C. Bond and S.F. Tahir, Appl. Catal. 71 (1991) 1 .
[7] C.L. Pieck, S. del Val, M. López Granados, M.A. Bañares and J.L.G. Fierro, Langmuir 18 (2002) 2642.
[8] I.E. Wachs and R.S. Saleh, U.S. Patent 4,582,912 (1986) to Exxon Res. & Eng.
[9] M. Felice, U.S. Patent 4,397,768 (1983) to Oxidaciones Organicas, C.A. ''OXIDOR''.
[10] Y. Nakanishi, Y. Akazawa, N. Ikeda and T. Suzuki, U.S. Patent 4,356,112 (1982) to Nippon Shukubai Kagaku Kogyo Co. Ltd.
[11] S.R. Dolhyi, E.L. Milberger and J.F. White, U.S. Patent 4,075,231 (1978) to The Standart Oil Co.
[12] T. Heidemann, H. Arnold, G. Hefele and H. Wanyek, U.S. Patent 6,362,345 (2002) to BASF Aktiengesellschaft.
[13] R.S. Saleh and I.E. Wachs, U.S. Patent 4,728,744 (1988) to Exxon Chem. Res. Co.
[14] J.M. Parera, Catal. Today 15 (1992) 481.
[15] M. Sanati, A. Andersson, L.R. Wallenberg and B. Rebenstorf, Appl. Catal., A 106 (1993) 51.
[16] A. Khodakov, J. Yang, S. Su, E. Iglesia and A.T. Bell, J. Catal. 177 (1998) 343.
[17] G. Balducci, P. Fornasiero and G. Graziani, Catal. Lett. 33 (1995) 193.
[18] C.G. Vayenas and S. Bebelis, Catal. Today 51 (1999) 581.
[19] T.J. Kim, Y.H. Kim and H.I. Lee, Hangop Hwahak 2 (1991) 330.
[20] H.B. Chiang and M.D. Lee, Appl. Catal., A 154 (1998) 55.
[21] J. Spengler, F. Anderle, E. Bosh, R.K. Graselli, B. Pillep, P. Behrens, O.B. Lapina, A.A. Shubin, H.-J. Eberle and H. Knoezinger, J. Phys. Chem. B 105 (2001) 10772.
[22] C.L. Pieck, M.A. Bañares, M.A. Vicente and J.L.G. Fierro, Chem. Mater. 13 (2001) 1174.
[23] S. del Val, M. López Granados, J.L.G. Fierro, J. Santamaría-González and A. Jiménez-López, J. Catal. 188 (1999) 203.
[24] JCPDS-International Center For Diffraction Data, Cards No. 13-307 and No. 24-1164, *Selected Power Diffraction Data For Metals and Alloys*, Data Book, 1st ed., Vol. II (Swarthmore, USA) .
[25] JCPDS-International Centre for Diffraction Data, Card No. 16-0422.
[26] JCPDS-International Centre for Diffraction Data, Card No. 21-1272.
[27] T. Birchall and A.W. Sleight, Inorg. Chem. 15 (1976) 868.

[28] S. Hansen, K. Ståhl, R. Nilsson and A. Andersson, J. Solid State Chem. 102 (1993) 340.
[29] G. Centi, P. Mazzoli and S. Perathoner, Appl. Catal., A 165 (1997) 273.
[30] JCPDS-International Centre for Diffraction Data, Card No. 32-0042.
[31] JCPDS-International Centre for Diffraction Data, Card No. 41-1426.
[32] R. Nilsson, T. Lindblad and A. Andersson, J. Catal. 148 (1994) 501.
[33] JCPDS-International Centre for Diffraction Data, Card No. 27-1318.
[34] JCPDS-International Centre for Diffraction Data, Card No. 31-1438.
[35] J. Miciukiewicz, T. Mang, and H. Knözinger, Appl. Catal., A 122 (1995) 151.
[36] G.T. Went, S.T. Oyama and A.T. Bell, J. Phys. Chem. 94 (1990) 4240.
[37] G. Deo and I.E. Wachs, J. Phys. Chem. 95 (1991) 5889.
[38] T.J. Dines, C.H. Rochester and A.M. Ward, J. Chem. Soc., Faraday Trans. 87 (1991) 653.
[39] M.A. Vuurman and I.E. Wachs, J. Phys. Chem. 96 (1992) 5008.
[40] I.E. Wachs, R.Y. Saleh, S.S. Chan and C.C. Chersich, Appl. Catal. 15 (1985) 339.